Inverse-Consistent Symmetric Free Form Deformation

Marc Modat[1], M. Jorge Cardoso[1], Pankaj Daga[1], David Cash[2], Nick C. Fox[2], and Sébastien Ourselin[1,2]

[1] Centre for Medical Imaging Computing, Department of Medical Physics and Bioengineering, University College London, UK
[2] Dementia Research Centre, Institute of Neurology, WC1N 3BG, University College London, UK

Abstract. Bias in image registration has to be accounted for when performing morphometric studies. The presence of bias can lead to unrealistic power estimates and can have an adverse effect in group separation studies. Most image registration algorithms are formulated in an asymmetric fashion and the solution is biased towards the transformation direction. The popular free-form deformation algorithm has been shown to be a robust and accurate method for medical image registration. However, it suffers from the lack of symmetry which could potentially bias the result. This work presents a symmetric and inverse-consistent variant of the free form deformation.

We first assess the proposed framework in the context of segmentation-propagation. We also applied it to longitudinal images to assess regional volume change. In both evaluations, the symmetric algorithm outperformed a non-symmetric formulation of the free-form deformation.

1 Introduction

Non-rigid image registration is a key component of many medical image analysis pipelines. Typically, when performing registration, a floating image is warped into the space of a reference image and the established spatial correspondences can be used to quantify changes through morphometric studies. Tensor-based morphometry, for example, is used to assess differences between different population whereas the Jacobian integration technique [1] aims at quantifying intra-patient longitudinal changes in specific regions of interest. Symmetry in registration is a desired property. Results should be the same when registration is performed from the first image to the second or from the second to the first image. In order to remove bias from the direction of registration, algorithms such as Symmetric Normalization (SyN) [2] from the Advanced Normalization Tools (ANTs[1]) package or the demons-based approaches by Tao *et al.* [3] or Vercauteren *et al.* [4] have been proposed. Bias in registration directionality has recently received a lot of attention and shown to generate unrealistic power estimates [5,6,7].

[1] `http://picsl.upenn.edu/ANTS`

B.M. Dawant et al. (Eds.): WBIR 2012, LNCS 7359, pp. 79–88, 2012.
© Springer-Verlag Berlin Heidelberg 2012

The Free-Form Deformation (FFD) algorithm [8] is a well-known and established method which has been found to perform well for inter-subject registration [9]. It has also been shown to be reliable for longitudinal intra-subject registration [1]. In the last decade, various improvements have been made to the original implementation in order to, for example, ensure one-to-one mapping between the registered scans using either soft constraints on the transformation Jacobian determinants [10] or using hard constraints in the form of boundary conditions [11,12]. The FFD approach is however lacking in symmetry, possibly causing bias towards the registration direction.

Feng *et al.* [13] presented work based on the FFD algorithm where they concurrently optimised a forward and backward transformation in order to minimise the sum of squared differences and a term based on the inverse consistency error [14]. Their implementation however could not be used for morphometric studies as they were only dealing with 2D images and they did not use any regularisation in order to enforce one-to-one correspondences. The proposed work expands the framework in order to obtain a symmetric inverse-consistent registration algorithm. Based on the FFD, we concurrently optimised the forward and backward transformations and penalised both transformations to ensure a one-to-one mapping and generate inverse-consistent and symmetric warping. The normalised mutual information (NMI) is used as a measure of similarity making the algorithm suitable for multi-modal registration.

We assessed our implementation using two datasets. The first part of the validation is based on segmentation-propagation where segmentations were propagated from one subject to another and were compared to manual segmentations that were performed on the same subject. The method was also validated by comparing brain atrophy measurement evaluated in several regions of interest.

2 Method

2.1 Classical Free-Form Deformation Approach

The FFD algorithm is a parametric approach for non-rigid registration of medical images [8]. The transformation $\mathbf{T}$ is parameterised by a regular lattice of control points $\{\boldsymbol{\mu}\}$ and a cubic B-Spline approximation scheme. The normalised mutual information (NMI) is used to assess the alignment between a reference image R and a floating image F after transformation $F(\mathbf{T})$. Maximising the NMI aims at maximising the amount of information that one image has about the other. In order to favor a smooth transformation, one or several penalty terms are added to the objective function. The bending energy (BE) is commonly used but one can also use other penalty terms, for example those based on the divergence of the transformation [15] or on the Jacobian determinant at every voxel position [10], the latter enabling an unfolded and invertible deformation.

2.2 Symmetric Transformation Model

A typical approach is to seek a transformation defined in the space of the reference image that warps the floating image to the reference image space. In order

to ensure symmetry, we propose to optimise two transformations: $\mathbf{T}_{Fw}$ and $\mathbf{T}_{Bw}$ where $\mathbf{T}_{Fw}$ is the forward transformation that maps the space of the reference image to the space of the floating image and $\mathbf{T}_{Bw}$ maps the space of the floating image to the space of the reference image. This joint optimisation should reduce directionality bias and increase capture range by using bi-directional gradient in the optimisation procedure.

2.3 Objective Function

In order to ensure inverse-consistency, as in Christensen [14], we used a penalty term based on the inverse-consistency error $\mathcal{P}_{IC}$:

$$\mathcal{P}_{IC} = \sum_{\boldsymbol{x}\forall R} \|\mathbf{T}_{Fw}(\mathbf{T}_{Bw}(\boldsymbol{x}))\|^2 + \sum_{\boldsymbol{x}\forall F} \|\mathbf{T}_{Bw}(\mathbf{T}_{Fw}(\boldsymbol{x}))\|^2 \tag{1}$$

A $\mathcal{P}_{IC}$ value of zero leads to the following equalities:

$$\mathbf{T}_{Fw} \approx \mathbf{T}_{Bw}^{-1} \text{ and } \mathbf{T}_{Bw} \approx \mathbf{T}_{Fw}^{-1}$$

The computation of the measure of similarity, NMI_{Sym}, also takes advantage of the forward and backward transformation:

$$\text{NMI}_{Sym} = \frac{H(R) + H(F(\mathbf{T}_{Fw}))}{H(R, F(\mathbf{T}_{Fw}))} + \frac{H(R(\mathbf{T}_{Bw})) + H(F)}{H(R(\mathbf{T}_{Bw}), F))}, \tag{2}$$

where $H(.)$ and $H(.,.)$ denote marginal and joint entropies respectively. Entropies are computed from two joint histograms filled using a Parzen windows approach [16]. The window we used here is a cubic B-Spline kernel.

In order to promote smoothness and to enforce topology conservation we used two other symmetric penalty terms based first on the BE:

$$\begin{aligned}\mathcal{P}_{BE} = & \sum_{\boldsymbol{x}\forall R} \left\| \frac{\partial^2 \mathbf{T}_{Fw}(\boldsymbol{x})}{\partial x^2} + \frac{\partial^2 \mathbf{T}_{Fw}(\boldsymbol{x})}{\partial y^2} + \frac{\partial^2 \mathbf{T}_{Fw}(\boldsymbol{x})}{\partial z^2} \right. \\ & \left. + 2 \times \left(\frac{\partial^2 \mathbf{T}_{Fw}(\boldsymbol{x})}{\partial xy} + \times \frac{\partial^2 \mathbf{T}_{Fw}(\boldsymbol{x})}{\partial yz} + \times \frac{\partial^2 \mathbf{T}_{Fw}(\boldsymbol{x})}{\partial xz} \right) \right\| \\ + & \sum_{\boldsymbol{x}\forall F} \left\| \frac{\partial^2 \mathbf{T}_{Bw}(\boldsymbol{x})}{\partial x^2} + \frac{\partial^2 \mathbf{T}_{Bw}(\boldsymbol{x})}{\partial y^2} + \frac{\partial^2 \mathbf{T}_{Bw}(\boldsymbol{x})}{\partial z^2} \right. \\ & \left. + 2 \times \left(\frac{\partial^2 \mathbf{T}_{Bw}(\boldsymbol{x})}{\partial xy} + \times \frac{\partial^2 \mathbf{T}_{Bw}(\boldsymbol{x})}{\partial yz} + \times \frac{\partial^2 \mathbf{T}_{Bw}(\boldsymbol{x})}{\partial xz} \right) \right\| \end{aligned} \tag{3}$$

and second on the determinant of the Jacobian matrices of the transformation:

$$\mathcal{P}_{Jac} = \sum_{\boldsymbol{x}\forall R} \log(|\text{Jac}(\mathbf{T}_{Fw}(\boldsymbol{x}))|)^2 + \sum_{\boldsymbol{x}\forall F} \log(|\text{Jac}(\mathbf{T}_{Bw}(\boldsymbol{x}))|)^2 \tag{4}$$

Note that the penalty term based on the inverse-consistency error does not guarantee folding-free transformations as the inverse-consistency error is minimised but not null.

The final objective function $\mathcal{O}(R, F; \boldsymbol{\mu}_{Fw}, \boldsymbol{\mu}_{Bw})$ to optimise is thus:

$$\begin{aligned}\mathcal{O}(R, F; \boldsymbol{\mu}_{Fw}, \boldsymbol{\mu}_{Bw}) = (1 - \alpha - \beta - \gamma) \times \mathrm{NMI}_{Sym} \\ + \alpha \times \mathcal{P}_{BE} + \beta \times \mathcal{P}_{Jac} + \gamma \times \mathcal{P}_{IC},\end{aligned} \tag{5}$$

where $\{\boldsymbol{\mu}_{Fw}\}$ and $\{\boldsymbol{\mu}_{Bw}\}$ correspond to the control point positions that define the transformation $\mathbf{T}_{Fw}$ and $\mathbf{T}_{Bw}$ respectively and $(\alpha + \beta + \gamma < 1)$

2.4 Optimisation

In order to optimise the objective function value, we used a conjugate gradient ascent approach. It requires the computation of the gradient of $\mathcal{O}$ according to each set of control points:

$$\frac{\partial \mathcal{O}(R, F; \boldsymbol{\mu}_{Fw}, \boldsymbol{\mu}_{Bw})}{\partial \boldsymbol{\mu}_F w} \text{ and } \frac{\partial \mathcal{O}(R, F; \boldsymbol{\mu}_{Fw}, \boldsymbol{\mu}_{Bw})}{\partial \boldsymbol{\mu}_B w}.$$

We refer the reader to [17] for an efficient computation of the NMI and BE derivatives and to [18] for the analytical derivative of the Jacobian-based penalty term. The derivatives of the inverse-consistency error penalty term are computed using a voxel-to-node approach where we first compute the derivative of each term at each voxel position and then concatenate the information at each control point position. We perform these computations by first computing four displacement fields through composition:

- $D1_R(\boldsymbol{x}) = \boldsymbol{x} - \mathbf{T}_{Fw}(\mathbf{T}_{Bw}(\boldsymbol{x}))$ where $\boldsymbol{x} \in R$
- $D2_R(\boldsymbol{x}) = \boldsymbol{x} - \mathbf{T}_{Bw}(\mathbf{T}_{Fw}(\boldsymbol{x}))$ where $\boldsymbol{x} \in R$
- $D1_F(\boldsymbol{x}) = \boldsymbol{x} - \mathbf{T}_{Fw}(\mathbf{T}_{Bw}(\boldsymbol{x}))$ where $\boldsymbol{x} \in F$
- $D2_F(\boldsymbol{x}) = \boldsymbol{x} - \mathbf{T}_{Bw}(\mathbf{T}_{Fw}(\boldsymbol{x}))$ where $\boldsymbol{x} \in F$

The residual displacement images $D1_R$ and $D2_R$ are then convolved by a cubic B-Spline kernel in order to reproduce the cubic B-Spline parametrisation of the $\mathbf{T}_{Fw}$ and the residual displacement images $D1_F$ and $D2_F$ are convolved by a kernel that reproduce the cubic B-Spline parametrisation of the $\mathbf{T}_{Bw}$. Using linear interpolation we then extract the gradient information at each control point position $\{\boldsymbol{\mu}_F w\}$ in $D1_R$ and $D2_R$ and at each control point position $\{\boldsymbol{\mu}_B w\}$ in $D1_F$ and $D2_F$

2.5 Implementation

The proposed algorithm has been implemented as part of the NiftyReg package, BSD licence, and can be downloaded from: `http://sourceforge.net/projects/niftyreg/`. Most symmetric registration implementations require the resampling

using a rigid or affine transformation of one image into the space of the other. This enables both images to have the same resolution making the computations easier. It could however bias the registration as different results are obtained depending to which image is interpolated. In the proposed implementation, both transformations $\mathbf{T}_{Fw}$ and $\mathbf{T}_{Bw}$ are defined in the original spaces of the input images and thus no prior resampling is required.

3 Evaluation

3.1 Segmentation Propagation

In order to evaluate the proposed algorithm, we first performed the cross-registration of 40 T1-weighted images from the LPBA40 database[2]. As in Klein *et al.* [9], we quantify the overlap between manually segmented regions of interest and segmentation propagated through registration. This experiment enables direct comparison to the 14 registration algorithms that have been evaluated by Klein *et al.* [9]. The LPBA40 database consists of 40 MRI and their associated brain parcellation into 56 regions of interest. LPBA40 images have been acquired using a 1.5T GE scanner and were used to generate a probabilistic atlas of the human cortical structures [19].

We used a block-matching approach for affine registration in order to initialise every registration [20]. Each non-rigid registration was performed using the proposed symmetric approach as well as using an asymmetric free-form deformation (FFD) implementation in NiftyReg. For every registration, we used a control point spacing of 2.5 millimetres along each axis. This spacing was chosen to replicate the image registration toolkit (IRTK[3]) parameters used in Klein *et al.*, as IRTK is also an FFD implementation. For the proposed approach, FFD-SYM, we set the weights of α ($\mathcal{P}_{BE}$), β ($\mathcal{P}_{Jac}$) and γ ($\mathcal{P}_{IC}$) in equation 5 to 1%, 1% and 10% respectively. The weights for FFD were set to 1% for α ($\mathcal{P}_{BE}$) and β ($\mathcal{P}_{Jac}$). Each registration was performed using a coarse-to-fine approach with 3 levels and the maximum number of iteration for each level was set to 1000.

Figure 1 presents the mean target overlap (TO) defined as:

$$\mathrm{TO} = \frac{1}{N} \sum_{i \forall k} \frac{\mathrm{GS}_k \cap \mathrm{PS}_k}{\mathrm{GS}_k}, \tag{6}$$

where GS_k and PS_k are the gold standard segmentation and the propagated segmentation, respectively, of the k^{th} region of interest and N is the number of regions of interest. The mean (std) target overlap values were 0.650 (0.022), 0.706 (0.025) and 0.714 (0.021) when performing the segmentation propagation using the affine transformation, FFD and the proposed symmetric approach respectively. The symmetric approach yielded significantly higher ($p < 10^{-4}$) target overlap values when compared to the non-symmetric free-form deformation.

[2] `http://www.loni.ucla.edu/Atlases/LPBA40`

[3] `http://www.doc.ic.ac.uk/~dr/software/`

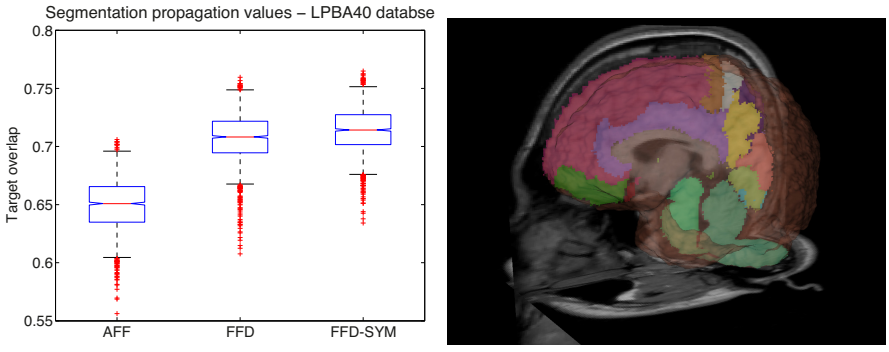

Fig. 1. Left-hand side: Segmentation propagation results. Target overlap are presented after affine registration and two different non-rigid registration approaches, a non-symmetric FFD implementation (FFD) and the proposed symmetric FFD scheme (FFD-SYM).

Right-hand side: Image S01 from the LPBA40 database and its corresponding parcelation.

3.2 Atrophy Measurement

The following experiments are based on a database that consists of T1-weighted MRI scans of 32 subjects with Alzheimer's disease (confirmed with histo-pathology) and 19 age-matched controls. We used three scans for each subject: two back-to-back scans at baseline and one follow-up scan after a year. The data acquisition was performed on a 1.5 T Signa Unit (GE Medical Systems, Milwaukee) with a inversion recovery (IR)-prepared spoiled GRASS sequence: TE 6.4 ms, TI 650 ms, TR 3000 ms, bandwidth 16 kHz, $256 \times 256 \times 128$ matrix with a field of view of $240 \times 240 \times 186$ mm. The first baseline scan and follow-up scan have four manual segmented structures: full brain (white matter plus grey matter), ventricles and left and right hippocampi.

Using the proposed symmetric approach and a non-symmetric FFD implementation, we registered every second baseline scan to its corresponding first baseline scan. As previously, the registrations were initialised using a block-matching technique for affine registration. In order to quantify the amount of deformation, we computed the mean and standard deviation of the Jacobian matrix determinants computed at every voxel position. The Jacobian determinant has the advantage of being unbiased towards any residual error of the initial global registration. The mean (std) in the full brain region of interest for FFD and FFD-SYM were 0.997 (0.006) and 0.998 (0.002) respectively and 0.986 (0.018) and 0.996 (0.011) in the hippocampi regions. Under the assumption that no changes should occur between same day scans, we observed smaller deformations using the proposed symmetric approach when compared to a non-symmetric approach, demonstrating the added value and robustness due to the inverse-consistent constrain.

For the next experiment we registered the first baseline scan of each patient to the corresponding follow-up scan. We also registered the follow-up scan to

the first baseline scan. For every registration we assessed the inverse-consistency error and computed the volume change for every region of interest using the integration of the Jacobian map over the regions of interest. We assessed the symmetry of the transformation by comparing the forward transformation from baseline to follow-up with the backward transformation from follow-up to baseline and comparing the backward transformation from baseline to follow-up with the forward transformation from follow-up to baseline. Table 1 presents the inverse-consistency error defined as the euclidean distance between the composition of the forward and backward transformation to the identity transformation.

Table 1. Inverse consistency error. Presented values have been computed from all longitudinal registrations using a non-symmetric (FFD) and a symmetric approach (FFD-SYM).

IC error (in mm)		Mean values over all subjects		
		mean($\overline{\text{IC}}$)	std($\overline{\text{IC}}$)	max($\overline{\text{IC}}$)
FFD	$\|T_{Fw}(T_{Bw}(\boldsymbol{x})) - \text{Id}\|$	0.6465	0.1012	0.8991
	$\|T_{Bw}(T_{Fw}(\boldsymbol{x})) - \text{Id}\|$	0.6498	0.1030	0.9005
FFD-SYM	$\|T_{Fw}(T_{Bw}(\boldsymbol{x})) - \text{Id}\|$	0.0696	0.0063	0.0864
	$\|T_{Bw}(T_{Fw}(\boldsymbol{x})) - \text{Id}\|$	0.0698	0.0063	0.0821

Due to order independent construction of the algorithm, no symmetric error was found up to numerical precision, using both single or double floating precision. The proposed method is thus order independent, as for every registration, the forward transformation from follow-up to baseline and backward transformation from baseline to follow-up are identical.

Figure 2 presents the volume changes from baseline to follow-up and follow-up to baseline computed on three regions of interest relevant to Alzheimerś disease: ventricles and hippocampi (left and right hippocampi have been merged into one figure).

In order to assess the symmetry of the method, we performed a one-sample t-test to compare the volume changes computed by registering follow-up to baseline and baseline to follow-up. The confidence intervals and their ranges are shown in table 2.

This confidence intervals show some degree of bias between the values obtained using both the forward and backward Jacobian integrations for every approach. It can however be noticed from the confidence interval that the bias is not only lower but also has a variability range one order of magnitude smaller when using the symmetric approach compared to the non-symmetric approach. Using the proposed symmetric method, the reduced bias towards chosen directionality and the reduced inverse-consistency error lead to an increase in registration robustness, as seen by the reduced number of outliers. It thus results in more realistic group separation estimates. Nonetheless, other sources of bias on both the pre-processing pipeline such as differential bias field and on the manual segmentations still require further investigation.

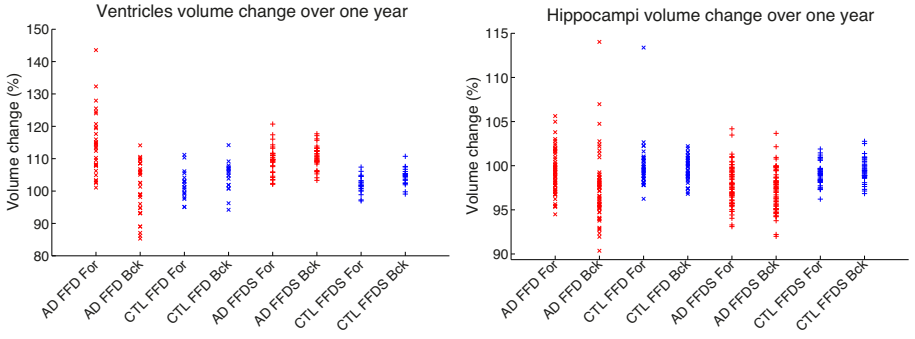

Fig. 2. Regions of interest volume change. The plots presents the volume changes from baseline to follow-up for three regions of interest: ventricles and both hippocampi. The volume changes have been estimated using a non-symmetric (FFD) and a symmetric (FFDS) registration approach and they have been estimated from the registration from follow-up to baseline (FOR) and from baseline to follow-up (BCK). The red and blue crosses correspond to volume change for Alzheimer's disease (AD) patients and for healthy control (CTL) respectively.

Table 2. Confidence intervals of the difference in longitudinal volume changes over the regions of interest estimated through Jacobian integration using both forward and backward transformations

		Ventricles	Hippocampi
FFD	95% CI	[2.2730 11.6473]	[0.6749 2.1020]
	CI range	8.2743	1.4271
FFD-SYM	95% CI	[-1.9593 -1.1673]	[0.0547 0.3497]
	CI range	0.7919	0.2950

4 Conclusion

We presented an extension of the work of Rueckert *et al.* [8] and Feng *et al.* [13] in order to register images without bias towards directionality. Our transformations, forward and backward, are both parameterised using a uniform cubic B-Spline and the normalised mutual information is used as a measure of similarity. The proposed framework has been implemented using a open-source package for registration and is thus available to download under a BSD licence

Using segmentation-propagation to evaluate the proposed method showed the added value of symmetry and inverse-consistency as it leads to increased overlap. We used longitudinal data in order to evaluate atrophy in multiple regions of interest. The proposed approach decreased bias towards the transformation direction when estimating volume changes compared to a non-symmetric approach sharing the same deformation model, regularisation and measure of similarity.

Future work will include a more extensive validation using larger cohort of patients. We also want to apply the proposed algorithm to tensor-based morphometry analysis to quantify the bias towards directionality as in Yushkevich *et al.* [21].

On a more methodological point of view, we will expand the framework to account for multiple time points (more than two) in a common registration framework.

Acknowlegment. The authors would like to thanks Dr Jonathan Schott for his help with the MIRIAD dataset and Tristan Clark for his assistance with the UCL computer science computer cluster. Marc Modat and Sebastien Ourselin were supported by CBRC grant 168. Pankaj Daga was funded by EPSRC-CRUK Comprehensive Cancer Imaging Centre of UCL and KCL (grant number C1519AO). Jorge M. Cardoso was funded by Fundacao para a Ciencia e a Tecnologia, Portugal. Nick C. Fox was employed by University College London Hospitals/University College London, which received a proportion of funding from the Department of Health's National Institute for Health Research Biomedical Research Centres funding scheme. The Dementia Research Centre is an Alzheimer's Research Trust Coordinating Centre and has also received equipment funded by the Alzheimer's Research Trust. Nick C. Fox is a MRC Senior Clinical Fellow and National Institute for Health Research Senior Fellow.

References

1. Boyes, R., Rueckert, D., Aljabar, P., Whitwell, J., Schott, J., Hill, D., Fox, N.: Cerebral atrophy measurements using Jacobian integration: Comparison with the boundary shift integral. Neuroimage 32(1), 159–169 (2006)
2. Avants, B.B., Epstein, C.L., Grossman, M., Gee, J.C.: Symmetric diffeomorphic image registration with cross-correlation: evaluating automated labeling of elderly and neurodegenerative brain. Medical Image Analysis 12(1), 26–41 (2008)
3. Tao, G., He, R., Datta, S., Narayana, P.A.: Symmetric inverse consistent nonlinear registration driven by mutual information. Comput. Meth. Prog. Bio. 95(2), 105–115 (2009)
4. Vercauteren, T., Pennec, X., Perchant, A., Ayache, N.: Symmetric Log-Domain Diffeomorphic Registration: A Demons-Based Approach. In: Metaxas, D., Axel, L., Fichtinger, G., Székely, G. (eds.) MICCAI 2008, Part I. LNCS, vol. 5241, pp. 754–761. Springer, Heidelberg (2008)
5. Thompson, W.K., Holland, D., Initiative, A.D.N.: Bias in tensor based morphometry stat-ROI measures result in unrealistic power estimates. NeuroImage 57(1), 1–4 (2011); discussion 5–14
6. Hua, X., Gutman, B., Boyle, C.P., Rajagopalan, P., Leow, A.D., Yanovsky, I., Kumar, A.R., Toga, A.W., Jack, C.R., Schuff, N., Alexander, G.E., Chen, K., Reiman, E.M., Weiner, M.W., Thompson, P.M.: Accurate measurement of brain changes in longitudinal MRI scans using tensor-based morphometry. NeuroImage 57(1), 5–14 (2011)
7. Fox, N.C., Ridgway, G.R., Schott, J.M.: Algorithms, atrophy and Alzheimer's disease: cautionary tales for clinical trials. NeuroImage 57(1), 15–18 (2011)
8. Rueckert, D., Sonoda, L., Hayes, C., Hill, D., Leach, M., Hawkes, D.: Nonrigid registration using free-form deformations: Application to breast MR images. IEEE Transactions on Medical Imaging 18(8), 712–721 (1999)

9. Klein, A., Andersson, J., Ardekani, B., Ashburner, J., Avants, B., Chiang, M., Christensen, G., Collins, D., Gee, J., Hellier, P., et al.: Evaluation of 14 nonlinear deformation algorithms applied to human brain MRI registration 46(3), 786–802 (July 2009)
10. Rohlfing, T., Maurer Jr., C.R., Bluemke, D.A., Jacobs, M.A.: Volume-preserving nonrigid registration of MR breast images using free-form deformation with an incompressibility constraints. IEEE Transactions on Medical Imaging 22(6), 730–741 (2003)
11. Rueckert, D., Aljabar, P., Heckemann, R.A., Hajnal, J.V., Hammers, A.: Diffeomorphic Registration Using B-Splines. In: Larsen, R., Nielsen, M., Sporring, J. (eds.) MICCAI 2006, Part II. LNCS, vol. 4191, pp. 702–709. Springer, Heidelberg (2006)
12. Sdika, M.: A fast nonrigid image registration with constraints on the Jacobian using large scale constrained optimization. IEEE Transactions on Medical Imaging 27(2), 271–281 (2008)
13. Feng, W., Reeves, S., Denney, T., Lloyd, S., Dell'Italia, L., Gupta, H.: A new consistent image registration formulation with a b-spline deformation model. In: Rosen, B., Brooks, D. (eds.) IEEE International Symposium on Biomedical Imaging: From Nano to Macro, pp. 979–982 (2009)
14. Christensen, G.E., Johnson, H.J.: Consistent image registration. IEEE Transactions on Medical Imaging 20(7), 568–582 (2001)
15. Ashburner, J., Friston, K.J.: Nonlinear spatial normalization using basis functions. Hum. Brain Mapp. 7(4) (June 1999)
16. Mattes, D., Haynor, D.R., Vesselle, H., Lewellen, T.K., Eubank, W.: PET-CT image registration in the chest using free-form deformations. IEEE Transactions on Medical Imaging 22(1), 120–128 (2003)
17. Modat, M., Ridgway, G.R., Taylor, Z.A., Lehmann, M., Barnes, J., Hawkes, D.J., Fox, N.C., Ourselin, S.: Fast free-form deformation using graphics processing units. Comput. Meth. Prog. Bio. 98(3), 278–284 (2010)
18. Modat, M., Ridgway, G.R., Daga, P., Cardoso, M.J., Ashburner, J., Ourselin, S.: Parametric non-rigid registration using a stationary velocity field. In: Zhou, S.K., Duncan, J.S., Ourselin, S. (eds.) IEEE Workshop on Mathematical Methods in Biomedical Image Analysis, MMBIA (2012)
19. Shattuck, D., Mirza, M., Adisetiyo, V., Hojatkashani, C., Salamon, G., Narr, K., Poldrack, R., Bilder, R., Toga, A.: Construction of a 3D probabilistic atlas of human cortical structures 39(3), 1064–1080 (February 2008)
20. Ourselin, S., Roche, A., Subsol, G., Pennec, X., Ayache, N.: Reconstructing a 3D structure from serial histological sections. Image and Vision Computing 19(1-2), 25–31 (2001)
21. Yushkevich, P.A., Avants, B.B., Das, S.R., Pluta, J., Altinay, M., Craige, C., Initiative, A.D.N.: Bias in estimation of hippocampal atrophy using deformation-based morphometry arises from asymmetric global normalization: an illustration in ADNI 3 T MRI data. NeuroImage 50(2), 434–445 (2010)